Bond-strength inversion in (In,Ga)As semiconductor alloys

Stefanie Eckner,[1,*] Konrad Ritter,[1] Philipp Schöppe,[1] Erik Haubold,[1] Erich Eckner,[2] Jura Rensberg,[1] Robert Röder,[1] Mark C. Ridgway,[3] and Claudia S. Schnohr[1]

[1]*Institut für Festkörperphysik, Friedrich-Schiller-Universität Jena, Max-Wien-Platz 1, 07743 Jena, Germany*
[2]*Institut für Optik und Quantenelektronik, Friedrich-Schiller-Universität Jena, Max-Wien-Platz 1, 07743 Jena, Germany*
[3]*Department of Electronic Materials Engineering, Research School of Physics and Engineering, The Australian National University, Canberra ACT 0200, Australia*

The atomic-scale structure and vibrational properties of semiconductor alloys are determined by the energy required for stretching and bending the individual bonds. Using temperature-dependent extended x-ray absorption fine-structure spectroscopy, we have determined the element-specific In-As and Ga-As effective bond-stretching force constants in (In,Ga)As as a function of the alloy composition. The results reveal a striking inversion of the bond strength where the originally stiffer bond in the parent materials becomes the softer bond in the alloy and vice versa. Our findings clearly demonstrate that changes of both the individual bond length and the surrounding matrix affect the bond-stretching force constants. We thus show that the previously used common assumptions about the element-specific force constants in semiconductor alloys do not reproduce the composition dependence determined experimentally for (In,Ga)As.

I. INTRODUCTION

Semiconductor alloys such as (In,Ga)As are frequently applied in state-of-the-art electronic and opto-electronic devices, including high-performance transistors [1,2], infrared detectors [3], high-efficiency solar cells [4], and nanolasers [5], since their key material properties can be specifically tailored by adjusting the alloy composition. Many of these properties depend on the bond lengths and bond strengths in the material and detailed knowledge of the bond-stretching force constants is crucial for a precise modeling and further enhancement of semiconductor devices. In particular, bond force constants characterize the response of a bond to stress or strain and thus determine the atomic-scale structure of alloys [6], thin films [7], interfaces [8], and nanostructures [9], thereby influencing their electronic and optical properties. Furthermore, the bond force constants are used to calculate phonon dispersion spectra [10,11] and impact vibrational and thermodynamic properties such as thermal conductivity [12–14] and negative thermal expansion [15].

While bond-stretching force constants of ordered compound semiconductors are accessible via macroscopic elastic constants [16], this approach fails for all random alloys. The resulting lack of experimental data led to contradicting assumptions about the composition dependence of the element-specific force constants in semiconductor alloys. When modeling the atomic-scale structure of semiconductor alloys and the resulting electronic and optical properties, the alloy force constants are usually assumed to be identical to those of the parent materials [6,17–19]. However, the element-specific bond lengths show a small but significant linear change with

alloy composition [6,20]. Studies of vibrational properties therefore typically assume that the strength of the bonds and thus the frequency of the oscillations change proportionally to this change in bond lengths [21,22], a law commonly referred to as Grüneisen relation. *Ab initio* finite-displacements calculations support the assumption of a linear relation between bond-stretching force constants and bond lengths for (In,Ga)As [23], but the proportionality factors differ substantially. Additionally, molecular dynamics simulations for (In,Ga)As [24] and first-principles calculations for (In,Ga)P [19] hint at a strong composition dependence of the force constants leading to a bond strength inversion. An independent experimental determination of the bond strengths in semiconductor alloys is thus required to evaluate the validity of typical assumptions and theoretical predictions about the fundamental properties of these highly relevant material systems.

Some insight into the composition dependence of the bond strengths in (In,Ga)As can be deduced from a comprehensive study of Raman-mode frequencies as a function of alloy composition [21]. The GaAs-like transversal optical (TO) mode in the alloy is well described by considering localization effects in addition to the Grüneisen relation. The InAs-like TO mode shows, in the Ga-rich compositional range, deviations from the expected behavior based on Grüneisen relation and localization effects [21]. They are interpreted as mode-coupling effects due to the overlap with GaAs-like optical modes. While these results document a clear composition dependence of the bond strengths, the complex relationship between single phonon mode frequencies and force constants for bond stretching and bond bending precludes the straightforward determination of alloy bond-stretching force constants from measured Raman modes.

---

*Corresponding author: Stefanie.Eckner@uni-jena.de

However, element-specific effective bond-stretching force constants can be determined experimentally for random alloy systems by temperature-dependent extended x-ray absorption fine-structure spectroscopy (EXAFS). Here we study the vibrational behavior of In-As and Ga-As bonds in (In,Ga)As as a function of alloy composition and we discuss the resulting bond-stretching force constants in the framework of both atomistic model simulations and vibrational spectroscopy studies.

II. EXPERIMENTAL

Powders of the binary materials GaAs and InAs were obtained from milled bulk wafers. Three (In,Ga)As random-alloy thin films were grown on InP using metal organic chemical vapor deposition. The thin-film quality and composition were determined using Rutherford backscattering spectroscopy and energy-dispersive x-ray analysis [25]. The films were covered with Apiezon black wax and the InP substrate beneath was removed using HCl(32%):H_2O [26,27]. The black wax was rinsed off with trichloroethylene and the thin film material was mixed with graphite powder and milled in a ball mill for 30 min. The sample material was then pressed to pellets approximately 1 mm thick, with an effective (In,Ga)As thickness of about 0.1 absorption lengths 50 eV above either the In or the Ga absorption edge, i.e., two pellets with different effective thicknesses were prepared for the ternary alloys [25].

Temperature-dependent EXAFS measurements were performed at the SuperXAS beamline at the Swiss Light Source (SLS) in Villigen, Switzerland. The spectra were recorded in fluorescence mode at the Ga and In-*K* edge (10367 eV and 27940 eV, respectively) applying nine different sample temperatures in the range from 35 K to 300 K. For selected temperatures, especially room temperature, up to three spectra were taken to confirm the reproducibility of the measurement.

III. DATA ANALYSIS

The data were processed and analyzed based on the cumulant expansion method [28] using the LARCH code [29] with phase shifts and scattering amplitudes calculated by FEFF9 [30]. The threshold energy E_0 was set to the average value determined from all samples measured at a given absorption edge. The coordination number was fixed to four, whereas the amplitude reduction factor S_0^2 was varied freely per sample in simultaneous fits of all spectra of this sample measured at a given absorption edge. The EXAFS signal was then fitted by refining the mean value d (bond length), the variance σ^2 (bond length variation), and the asymmetry parameter C_3 of the element-specific nearest-neighbor distance distribution.

The distance distribution originates mostly from thermal vibrations of the atoms relative to each other. Therefore, its width (represented by σ^2) usually increases with increasing temperature as shown in Fig. 1. In principle, the temperature dependence of σ^2 can be approximated by either the correlated Einstein or the correlated Debye model. The correlated Einstein model [25,31,32] is simpler, well suited for materials with zinc-blende structure, and has been successfully applied to describe vibrational properties in a range of binary III-V and II-VI semiconductors [9,32–34]. As seen in Fig. 1 and the Supplemental Material [25], the variance σ^2 of the distance distribution is well represented by the Einstein model
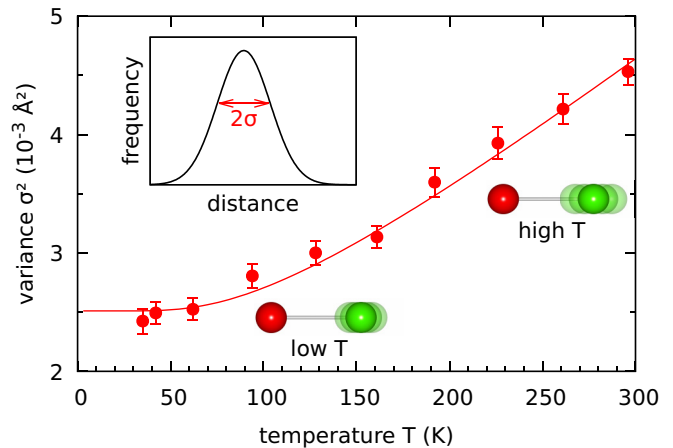

FIG. 1. Temperature dependence of the variance σ^2 of the nearest-neighbor distance distribution (symbols) and fit with a correlated Einstein model (solid line) for the In-As bond in $In_{0.5}Ga_{0.5}As$. The inset shows a schematic of the distance distribution, resulting mostly from thermal vibrations of the atoms relative to each other.

curves also for ternary (In,Ga)As alloys. In the harmonic approximation [32], the expression for σ^2 includes two free parameters, namely the bond-stretching force constant k and a temperature-independent constant σ_{st}^2. The former describes thermal vibrations, which increase with increasing temperature, while the latter represents static disorder caused by strain or alloying [25]. The bond-stretching force constants obtained from temperature-dependent EXAFS measurements are typically smaller than the bond-stretching force constants 3α calculated from macroscopic elastic properties [6]. A small difference is not surprising, though, given that temperature-dependent EXAFS probes dynamic properties while elastic constants describe the static behavior of the material under stress and strain.

The asymmetry parameter C_3, which also increases with increasing temperature, was described using the corresponding Einstein model expression with terms to third order [31], yielding values up to 10^{-4}Å^3 at room temperature in good agreement with previous work [33,35]. All higher cumulants were set to zero because a full anharmonic fit using the fourth-order terms up to the fourth cumulant [36] showed no significant difference of the resulting bond-stretching force constants but strongly reduced the stability of the fit. For each sample and type of bond, an extensive set of fits was performed with a systematic variation of the analysis parameters and settings to estimate the overall uncertainties of the resulting bond-stretching force constants as shown in Fig. 2. The tests included variation of the background subtraction parameters (edge energy and rbkg parameter in LARCH), the window function for Fourier transformation (k_{min}, k_{max}, tapering parameter dk, and weighting exponent kw), the fitting range (r_{min}, r_{max}, and tapering parameter dr), and the model used in the fit (different assumptions for threshold energy and amplitude reduction factor, inclusion of anharmonic contributions, and inclusion of second- and third-nearest neighbor scattering paths with different parametrizations). Furthermore, data analysis using the ratio method [28] was done for comparison and yields the same compositional trends.
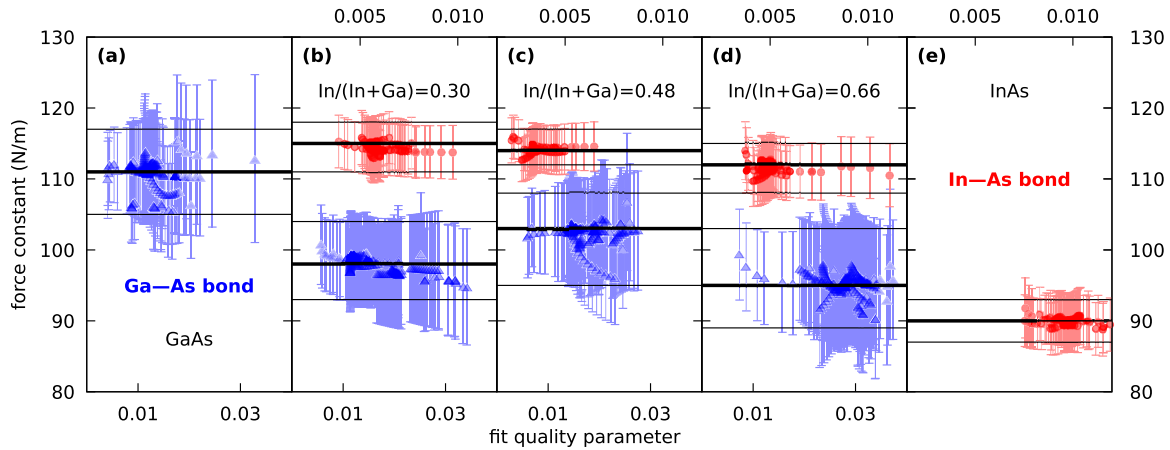
FIG. 2. The effective bond-stretching force constants obtained from different Einstein model fits are plotted as a function of the fit quality parameter R for the In-As bond (red circles, top axis) in all In-containing samples and the Ga-As bond (blue triangles, bottom axis) in all Ga-containing samples. More than 150 fits were performed for each sample at a given absorption edge with a systematic variation of the analysis parameters, including parameters for the background subtraction, the Fourier transform window, the fitting range, and the fit model, to estimate the effect of these parameters on the bond-stretching force constants. The error bars plotted are the uncertainties reported for the different fits. The final values (thick black lines) are the results from one particular fit that yields good agreement with the data for all samples. The final uncertainties (thin black lines) are determined from the variation of all test results and thus include all uncertainties arising from a variation of the data processing and the fit procedure.

IV. RESULTS

The effective bond-stretching force constants for the Ga-As and In-As bonds are plotted as a function of the alloy composition in Fig. 3 (full symbols). A k_{Ga-As} value of 111 N/m is obtained for GaAs in excellent agreement with
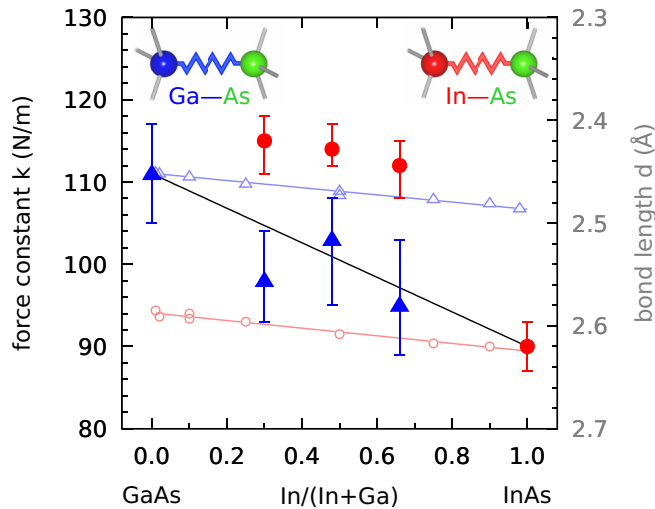

FIG. 3. Element-specific effective bond-stretching force constants k (left axis) of the Ga-As (full blue triangles) and In-As (full red circles) bonds in (In,Ga)As as a function of alloy composition. The uncertainties were determined through systematic variation of the fitting procedure (see Fig. 2 and Sec. III). A linear change between the binary values (black dashed line) is predicted by *ab initio* calculations [23] based on the element-specific Ga-As and In-As bond lengths d (open blue triangles and open red circles, respectively) measured with EXAFS [20]. The latter are shown on an inverted scale (right axis) since an increase of the bond lengths leads to a reduction of the force constants.

previous EXAFS studies [33]. For InAs, a k_{In-As} value of 90 N/m is obtained in accordance with the empirical law that an increase in bond length (2.448 Å for GaAs and 2.623 Å for InAs [6]) is accompanied by a decrease of the bond-stretching force constant [37]. The Ga-As bonds are thus clearly stiffer than the In-As bonds in their respective binary materials.

Strikingly, the bonds of the ternary materials show an entirely different behavior. The experimentally determined effective bond-stretching force constants of the In-As bonds are significantly larger than those of the Ga-As bonds. This relation is supported by molecular dynamics calculations for (In,Ga)As, which show a small positive deviation of the lattice constant from Vegard's law [24]. First-principles calculations of $In_{0.5}Ga_{0.5}P$ show a pronounced inversion of the bond-stretching parameters, which were determined by fitting a valence force field model to the calculated macroscopic elastic constants [19]. Comparing the experimentally determined force constants in $In_{0.5}Ga_{0.5}As$ to GaAs and InAs reveals a decrease of k_{Ga-As} by approximately 10% and an increase of k_{In-As} by almost 30%. Furthermore, the change is obviously not linear with alloy composition for the In-As bond. Consequently, both models used so far, namely the simple model of composition-independent force constants used in structural modeling [6,17,18] and the linear dependence assumed in vibrational spectroscopy studies [21,22] cannot explain the experimental findings. Instead, the element-specific force constants of (In,Ga)As exhibit a strong and for the In-As bond nonlinear dependence on the alloy composition, including a remarkable inversion of the Ga-As and In-As bond strengths.

V. DISCUSSION

These astonishing results can be discussed in the framework of two opposing approaches: The local bond picture used in atomic-scale structural calculations considers a single bond embedded in a matrix. The extended mode picture applied
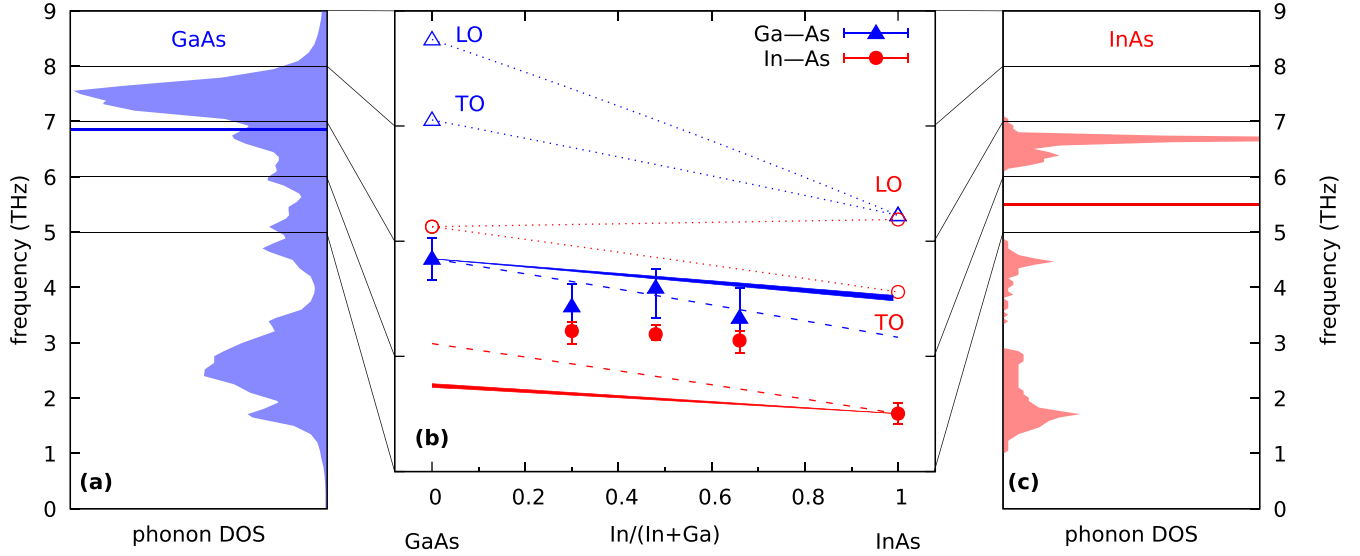
FIG. 4. Phonon density of states (shaded area) of (a) GaAs [38] and (c) InAs [39]. Panel (b) shows the element-specific Einstein frequencies (full symbols) determined in this paper together with the frequencies of Raman optical modes (open symbols and dotted lines) [21] for (In,Ga)As as a function of alloy composition. The theoretical prediction according to the Grüneisen relation (solid area) and a linear interpolation between the binary force constants (dashed lines) are also shown. The binary values of the Einstein frequencies are further included in (a) and (c) (thick solid lines).

for vibrational spectroscopy studies considers collective vibrations involving a given bond species in the crystal. For both approaches, our results reveal the fundamental role of processes up to now often neglected in the description of ternary semiconductor alloys.

A. Local bond picture

In the local bond picture, the observed *effective* force constant k differs from the *intrinsic* force constant of an isolated bond because the matrix surrounding the bond influences its elastic response and vibrational behavior. All force constants determined experimentally or theoretically for solids are thus effective force constants. They will change if the intrinsic force constants are modified by bond-length changes or by charge redistribution between the atoms. Adopting the empirical law valid for binary III-V materials [37], the slight increase of the bond lengths with alloy composition [6,20] shown in Fig. 3 (open symbols and inverted right axis) would give rise to a 2% decrease or increase of k_{Ga-As} or k_{In-As}, respectively, when going from the binary materials to $In_{0.5}Ga_{0.5}As$. This is significantly less than the change of 10% and 30% observed in Fig. 3 for our experimental values. Consequently, the mixed matrix in the alloy system plays a crucial role in determining the effective bond-stretching force constants and k is affected by the exchange of atoms in the matrix with changing alloy composition. Successive substitution of Ga with In atoms shifts the average intrinsic force constants of the adjacent bonds from the Ga-As to the In-As value. Moreover, the increasing bond lengths with increasing indium content lead to a softening in the force constants of the matrix. In a softer matrix, the relaxation and vibration of the bond under consideration is less restricted by the surrounding crystal, which reduces the effective force constant k.

Ab initio finite-displacements calculations in 64-atom (In,Ga)As supercells suggest that the influence of the matrix

conserves the strict correlation between force constant k and bond length d [23]. The relation is linear with approximately the same slope for k_{Ga-As} and k_{In-As}, but it differs substantially from the empirical law for binary III-V materials [37]. Using the known composition dependence of the bond lengths [6,20], the estimated bond-stretching force constants lie on a straight line between the binary values (black dashed line in Fig. 3). While this prediction is consistent with the experimental values for k_{Ga-As}, it does not reproduce the experimental k_{In-As}, possibly due to dynamic contributions not covered by the static finite-displacements method.

Consequently, our results demonstrate that the assumption of composition-independent force constants commonly used within the local bond picture is clearly not adequate. Instead, the modification of both (i) the individual bond (bond length changes and charge redistributions) and (ii) the surrounding matrix (softening or stiffening due to an exchange of neighboring atoms) leads to a significant difference between the effective bond-stretching force constants k in the ternary alloys compared to the binary compounds.

B. Extended mode picture

The extended mode picture focuses on collective vibrations in the form of phonon modes. In the Einstein model, the bond-stretching force constant k is directly related to the Einstein frequency ν, which is a single frequency approximation of the complex phonon spectrum as depicted in Fig. 4(a) for GaAs and Fig. 4(c) for InAs. The Einstein frequencies of (In,Ga)As, depicted as full symbols in Fig. 4(b), decrease with increasing indium content, while ν_{Ga-As} is larger than ν_{In-As} over the whole compositional range. The dashed black line in Fig. 3 transforms into two distinct red and blue dashed lines in Fig. 4(b), because ν is related to k via the reduced mass of the

bond. Thus, equal force constants for Ga-As and In-As bonds would still correspond to different Einstein frequencies.

For comparison, the longitudinal optical (LO) and TO modes measured with Raman spectroscopy [21] are added in Fig. 4(b) as open symbols and dotted lines. While these single phonon modes are easily accessible, they cannot be used to extract bond-stretching force constants in a simple way, since their frequency is also dependent on bond-bending forces [18,40], localization effects [21,22,41], and mode coupling [21,22]. According to the Grüneisen relation, an increase of the bond length leads to a reduction of the corresponding mode frequency. Consequently, most optical mode frequencies in Fig. 4(b) decrease with increasing indium content.

In addition to the bond length dependence, the mode frequencies in alloy systems are affected by localization effects due to the different bond species present in the material. If the difference of frequencies for different modes is large enough, each Raman mode is confined to one bond species. The number of a particular bond species decreases with decreasing content of the element involved and the respective bonds become more isolated in nature. This leads to a spatial localization of the Raman mode in question, weakening the rule of vanishing phonon momentum. Consequently, the volume of the Brillouin zone probed by the measurement is enlarged, thereby shifting the mode frequency in materials with significant phonon dispersion [21,22,41].

In (In,Ga)As, the composition dependence of the GaAs-like TO mode is well accounted for by bond length changes applying the Grüneisen relation and by a change of the vibrational behavior due to localization effects in the ternary alloy [21]. In contrast, the InAs-like mode deviates from the expected behavior, especially in the Ga-rich composition range, which can be attributed to mode coupling caused by the frequency overlap with GaAs-like modes. This interpretation is supported by the data for the InAs-like TO mode in In(As,P), where the frequency overlap is absent and the composition dependence of the mode frequency is well described by bond-length changes and localization effects [21].

An effective Raman force constant can be calculated by formally applying the relation between force constant k and vibrational frequency ν to the Raman TO mode frequencies. The resulting values follow the relationship $k_{\text{Ga−As}}^{\text{TO}} > k_{\text{In−As}}^{\text{TO}}$ for the Ga-rich limit and $k_{\text{Ga−As}}^{\text{TO}} < k_{\text{In−As}}^{\text{TO}}$ for the In-rich limit, which could be interpreted as an indication for a bond strength inversion in (In,Ga)As alloys. However, such an interpretation should be taken with great care since the Raman TO frequencies depend on bond-stretching and bond-bending force constants as well as on localization effects and mode coupling as discussed above.

Applying the Grüneisen relation to the Einstein frequencies by using the mode Grüneisen parameters of the LO or TO modes [42] yields the trend depicted in Fig. 4(b) as narrow solid regions. Clearly, only a small part of the composition dependence of the Einstein frequencies is thus accounted for. The discrepancy partly stems from the fact that EXAFS probes both optical and acoustic modes with very different Grüneisen parameters. Furthermore, the nonlinear characteristics of the measured $k_{\text{In−As}}$ values provide evidence for basic changes of the vibrational behavior of the atoms in the alloy system.

Localization effects involving differing contributions from the phonon dispersion as described above for the Raman modes do not occur for the Einstein frequencies determined with EXAFS since the sampled phonon spectrum involves the entire Brillouin zone from the start. However, other localization effects might occur such as reduction of restoring forces when neighboring atoms do not follow the antiphase oscillation [43], thereby decreasing the frequency of optical modes. Additionally, the overlap of the phonon spectra leads to coupling effects, so that acoustic modes, in particular, are not restricted to one bond species. Such mode coupling of nearby frequencies causes the transfer of oscillator strength to either lower or higher frequencies [22] and therefore shifts the average value.

In contrast to the commonly assumed proportionality between bond length and bond strength changes, our study clearly shows that the composition dependence of the Einstein frequencies within the extended mode picture is caused by an alteration of both (i) the individual bonds (bond length changes and charge redistributions) and (ii) their vibrational behavior (mode coupling and phonon localization).

VI. CONCLUSION

In conclusion, the relation between the composition of a semiconductor alloy and its element-specific effective bond-stretching force constants or Einstein frequencies is far from trivial, as evidenced in both the local bond picture and the extended mode picture. Furthermore, care must be taken when comparing force constants or vibrational frequencies obtained from different methods, even for materials with dominant optical modes. The experimental bond-stretching force constants of (In,Ga)As show a significant change with changing composition and exhibit a remarkable bond-strength inversion when compared to the parent materials GaAs and InAs. As a consequence, the force constants of semiconductor alloys cannot simply be taken as those of the binary parent compounds, nor can they be estimated solely based on the change of the bond lengths. In contrast, detailed knowledge of the composition-dependent strength of the different bond species present in the alloys is essential for a precise modeling of their structural, vibrational, electrical, and optical properties.

[1] J. A. del Alamo, Nature **479**, 317 (2011).

[2] K. Tomioka, M. Yoshimura, and T. Fukui, Nature **488**, 189 (2012).

[3] G. Ariyawansa, C. J. Reyner, J. M. Duran, J. D. Reding, J. E. Scheihing, and E. H. Steenbergen, Appl. Phys. Lett. **109**, 021112 (2016).

[4] M. A. Green and S. P. Bremner, Nat. Mater. **16**, 23 (2017).

[5] R. Chen, T.-T. D. Tran, K. W. Ng, W. Son Ko, L. C. Chuang, F. G. Sedgwick, and C. Chang-Hasnain, Nat. Photonics **5**, 170 (2011).

[6] C. S. Schnohr, Appl. Phys. Rev. **2**, 031304 (2015).

[7] J. C. Woicik, Surf. Sci. Rep. **69**, 38 (2014).

[8] M. Stengel, D. Vanderbilt, and N. A. Spaldin, Nat. Mater. **8**, 392 (2009).

[9] B. Gilbert, F. Huang, H. Zhang, G. A. Waychunas, and J. F. Banfield, Science **305**, 651 (2004).

[10] A. R. Overy, A. B. Cairns, M. J. Cliffe, A. Simonov, M. G. Tucker, and A. L. Goodwin, Nat. Commun. **7**, 10445 (2016).

[11] A. R. Overy, A. Simonov, P. A. Chater, M. G. Tucker, and A. L. Goodwin, Phys. Status Solidi B **254**, 1600586 (2017).

[12] C. W. Li, J. Hong, A. F. May, D. Bansal, S. Chi, T. Hong, G. Ehlers, and O. Delaire, Nat. Phys. **11**, 1063 (2015).

[13] M. N. Luckyanova, J. Garg, K. Esfarjani, A. Jandl, M. T. Bulsara, A. J. Schmidt, A. J. Minnich, S. Chen, M. S. Dresselhaus, Z. Ren, E. A. Fitzgerald, and G. Chen, Science **338**, 936 (2012).

[14] J. Ma, O. Delaire, A. F. May, C. E. Carlton, M. A. McGuire, L. H. VanBebber, D. L. Abernathy, G. Ehlers, T. Hong, A. Huq, W. Tian, V. M. Keppens, Y. Shao-Horn, and B. C. Sales, Nat. Nanotechnol. **8**, 445 (2013).

[15] J. T. Schick and A. M. Rappe, Phys. Rev. B **93**, 214304 (2016).

[16] R. M. Martin, Phys. Rev. B **1**, 4005 (1970).

[17] A. Balzarotti, N. Motta, A. Kisiel, M. Zimnal-Starnawska, M. T. Czyznyk, and M. Podgórny, Phys. Rev. B **31**, 7526 (1985).

[18] Y. Cai and M. F. Thorpe, Phys. Rev. B **46**, 15879 (1992).

[19] K. Biswas, A. Franceschetti, and S. Lany, Phys. Rev. B **78**, 085212 (2008).

[20] J. C. Mikkelsen, Jr. and J. B. Boyce, Phys. Rev. Lett. **49**, 1412 (1982).

[21] J. Groenen, R. Carles, G. Landa, C. Guerret-Piécourt, C. Fontaine, and M. Gendry, Phys. Rev. B **58**, 10452 (1998).

[22] R. Hajj Hussein, O. Pagès, S. Doyen-Schuler, H. Dicko, A. V. Postnikov, F. Firszt, A. Marasek, W. Paszkowicz, A. Maillard, L. Broch, and O. Gorochov, J. Alloy. Compd. **644**, 704 (2015).

[23] A. Nassour, J. Hugel, and A. V. Postnikov, J. Phys.: Conf. Ser. **92**, 012139 (2007).

[24] P. S. Branicio, J. P. Rino, F. Shimojo, R. K. Kalia, A. Nakano, and P. Vashishta, J. Appl. Phys. **94**, 3840 (2003).

[25] See Supplemental Material http://link.aps.org/supplemental/10.1103/PhysRevB.97.195202 for sample characterization and data analysis details.

[26] Z. S. Hussain, E. Wendler, W. Wesch, G. J. Foran, C. S. Schnohr, D. J. Llewellyn, and M. C. Ridgway, Phys. Rev. B **79**, 085202 (2009).

[27] S. Decoster, C. J. Glover, B. Johannessen, R. Giulian, D. J. Sprouster, P. Kluth, L. L. Araujo, Z. S. Hussain, C. S. Schnohr, H. Salama, F. Kremer, K. Temst, A. Vantomme, and M. C. Ridgway, J. Synchr. Rad. **20**, 426 (2013).

[28] G. Dalba and P. Fornasini, J. Synchr. Rad. **4**, 243 (1997).

[29] M. Newville, J. Phys.: Conf. Ser. **430**, 012007 (2013).

[30] J. J. Rehr, J. J. Kas, F. D. Vila, M. P. Prange, and K. Jorissen, Phys. Chem. Chem. Phys. **12**, 5503 (2010).

[31] T. Yokoyama, J. Synchr. Rad. **6**, 323 (1999).

[32] C. S. Schnohr, P. Kluth, L. L. Araujo, D. J. Sprouster, A. P. Byrne, G. J. Foran, and M. C. Ridgway, Phys. Rev. B **79**, 195203 (2009).

[33] S. I. Ahmed, G. Aquilanti, N. Novello, L. Olivi, R. Grisenti, and P. Fornasini, J. Chem. Phys. **139**, 164512 (2013).

[34] P. Fornasini and R. Grisenti, J. Synchr. Rad. **22**, 1242 (2015).

[35] P. Fornasini, R. Grisenti, M. Dapiaggi, G. Agostini, and T. Miyanaga, J. Chem. Phys. **147**, 044503 (2017).

[36] J. Haug, A. Chassé, R. Schneider, H. Kruth, and M. Dubiel, Phys. Rev. B **77**, 184115 (2008).

[37] A. S. Verma, Phys. Lett. A **372**, 7196 (2008).

[38] M. Durandurdu and D. A. Drabold, Phys. Rev. B **66**, 045209 (2002).

[39] P. H. Borcherds and K. Kunc, J. Phys. C: Solid State **11**, 4145 (1978).

[40] R. Vogelgesang, A. K. Ramdas, S. Rodriguez, M. Grimsditch, and T. R. Anthony, Phys. Rev. B **54**, 3989 (1996).

[41] O. Pagès, T. Tite, K. Kim, P. A. Graf, O. Maksimov, and M. C. Tamargo, J. Phys.: Condens. Mat. **18**, 577 (2006).

[42] S. Adachi, *Properties of Group IV, III-V and II-VI Semiconductors* (John Wiley & Sons, Chichester, 2005).

[43] H. Rücker and M. Methfessel, Phys. Rev. B **52**, 11059 (1995).